

# Bio-inspired leaf stent for direct treatment of cerebral aneurysms: design and finite element analysis

Xiang Zhou<sup>1</sup>, Zhong You\*<sup>1</sup> and James Byrne, M.D.<sup>2</sup>

<sup>1</sup>Department of Engineering Science, University of Oxford, UK, OX3 7DQ

<sup>2</sup>Department of Neuroradiology, Nuffield Department of Surgery, University of Oxford, UK, OX3 9DU

(Received August 5, 2010, Accepted August 28, 2010)

**Abstract.** Cerebral aneurysm is common lesion among adult population. Current methods for treating the disease have several limitations. Inspired by fern leaves, we have developed a new stent, called leaf stent, which can provide a tailored coverage at the neck of an aneurysm and thus prevent the blood from entering the aneurysm. It alone can be used to treat the cerebral aneurysm and therefore overcomes problems existing in current treating methods. The paper focuses on the numerical simulation of the leaf stents. The mechanical behaviour of the stent in various designs has been investigated using the finite element method. It has been found that certain designs provide adequate radial force and have excellent longitudinal flexibility. The performance of certain leaf stents is comparable and even superior to those of the commercially available cerebral stents such as the Neuroform stent and the Enterprise stent, commonly used for stent assisted coiling, while at the same time, providing sufficient coverage to isolate the aneurysm without using coils.

**Keywords:** cerebral aneurysm; leaf stent; nitinol; FEA (or finite element analysis); radial force; longitudinal flexibility; stent-artery interaction.

---

## 1. Introduction

Cerebral aneurysm is a weak region in the wall of an artery in the brain, where dilation or ballooning of the artery wall may occur. Its rupture can lead to fatal hemorrhages in the brain. Cerebral aneurysms are common lesions. In the United States alone more than 10 million people have intracranial aneurysms (Brisman *et al.* 2006). About 27000 of them suffer from ruptures of intracranial aneurysms each year, 10% of whom die before they reach the hospital (Wijdicks *et al.* 2005).

Current methods for treating intracranial aneurysms include surgical clipping and endovascular coiling (Mitha and Ogilvy 2005). In the surgical clipping method, the skull of the patient is opened, and a surgical clip is placed across the neck of the aneurysm to stop blood from flowing into the aneurysm sac. The risk of this method is relatively high, especially for elderly or medically complicated patients. Endovascular coiling procedure is a minimum invasive method involving placement of one or more coils, delivered through a catheter, into the aneurysm until the sac of the aneurysm is completely packed with coils. It helps to trigger a thrombus inside the aneurysm. Although endovascular coiling is commonly recognized to be safer than surgical clipping, it has its own limitations. First, the coils

---

\*Corresponding Author, P.h.D., E-mail: [zhong.you@eng.ox.ac.uk](mailto:zhong.you@eng.ox.ac.uk)

will remain permanently inside the aneurysm sac and roughly maintain its original size. As a result, the pressure exerted on the surrounding tissue of the aneurysm will not be removed. Second, this procedure is effective for the aneurysm that involves a well-formed sac with a small entrance neck. When used to treat the wide-neck aneurysm, the coil is likely to protrude into the parent vessels. A solution to prevent coil protrusion is to use a stent in combination with coiling embolization, called the stent-assisted coiling procedure. It involves first placing a stent across the aneurysm neck, serving as a scaffold inside the lumen. Then, the coils are delivered into the sac of the aneurysm through the interstices of the stent. Although this method can solve some problems associated with the coiling embolization, some drawbacks still remain. First, a microcatheter through which the coils are sent into the aneurysm sac has to be navigated through the interstices of the stent. This process is difficult and time-consuming. Second, the coils are still used to fill the sac of the aneurysm. As a result, the aneurysm size remains the same after the treatment. Furthermore, when it comes to the pseudoaneurysm where no fully-formed aneurysm sac can be identified, coiling methods are not applicable (Fiorella *et al.* 2006).

Using a stent alone to treat the aneurysm therefore becomes a promising way to avoid the problems stated above. In this method, a stent with an area of coverage is placed across the aneurysm neck, blocking it sufficiently to restrain blood from flowing into the sac and finally to trigger a thrombus within the aneurysm. Because the aneurysm solidifies naturally on itself, there is no danger of its rupture. Furthermore, because no coil is involved in this method, the aneurysm will gradually shrink as the thrombus is absorbed. Consequently, the pressure applied on the surrounding tissue can be removed.

The reason why this method has not been used is because of the difficulty in designing stent. It has to be flexible enough to pass through and morph the very tortuous blood vessel in brain whereas at the same time to provide sufficient coverage to shut the aneurysm. Current stents made for the stent-assisted coiling, such as the Neuroform stent made by Boston Scientific, the LEO stent by Balt of France, and the Enterprise stent by Corids, have a very open design in order to allow the coils to pass through the interstices and to achieve flexibility. They do not provide much coverage at all. Therefore, they are inadequate for direct treatment of the aneurysm.

The cover tubular stents cannot be directly used, too, due to its lack of good flexibility. Even if it could be used, a completely covered stent will also unavoidably block the small branch blood vessels, causing other clinical complications.

Research has shown that partially blocking the entrance to aneurysm can effectively prevent blood from entering the aneurysm (Kim *et al.* 2008). Therefore, the idea of covering the aneurysm by overlapping flexible materials seems to be a good option because it can be tailored to provide sufficient coverage only at required areas and more importantly such design leads to greater structural flexibility.

Inspired by the lace fern branches, we have developed a new stent, referred to as *the leaf stent*, for the direct treatment of the intracranial aneurysms (Zhou *et al.* 2009). The stent has sufficient amount of dense areas to provide adequate coverage to the neck of the aneurysm while retaining flexibility and conformability so that it can be easily navigated through tortuous arteries and adopt the path of the vessel after placement. The stent is made from nitinol. Moreover, the covered area can be tailored in order to serve as a right patch in the vicinity of the neck of the aneurysm, and the remainder of the stent can adopt a very open design to prevent blockage of the branch arteries adjacent to the aneurysm.

The focus of this paper is on performance assessment of the leaf stent using the finite element analysis (FEA) method. The layout of the paper is as follows. The design of the leaf stent is introduced

in Section 2. Section 3 deals with the materials properties and the FEA model of the stent. The comparison of the results with other related stents is given in Section 4. Section 5 contains conclusions and possible future work, which ends the paper.

## 2. Design of the leaf stent

A lace fern branch consists of a main stem with many small dissecting leaves, see Fig. 1. When it is pulled through a circular tube, the leaves overlap, adopting well the cylindrical profile even when the tube is curved. The leaf stent utilises the structural design of a fern branch. It has a tubular profile once it is expanded. Its basic element is a ring consisting of a zig-zag closed chain linkage attached with flexible leaves. Fig. 2 shows a plan view of an expanded single ring of the leaf stent notionally unwrapped from its actual tubular shape into a flat shape. It can be observed that the ring comprises a plurality of leaf components *a* interconnected by linkage components *b*. The linkage components are connected together forming a zigzag closed chain, with the leaves components each connected thereto. The reason to have a zigzag ring is to facilitate packaging. A number of such rings are connected longitudinally to form the stent. The packaging is achieved by folding the zig-zag chain linkage while wrapping the leaves around the folded frame core. To better illustrate the folding mechanism, a schematic diagram of the packaging of the ring is shown in Fig. 3. As the leaf components move in the circumferential direction *C* during folding, they slide over each other to move between the expanded state in which they do not overlap and the collapsed state in which they overlap. The stent is manufactured from a thin tube cut to define the leaf and linkage components. In the design shown in Fig. 2, the leaf components are

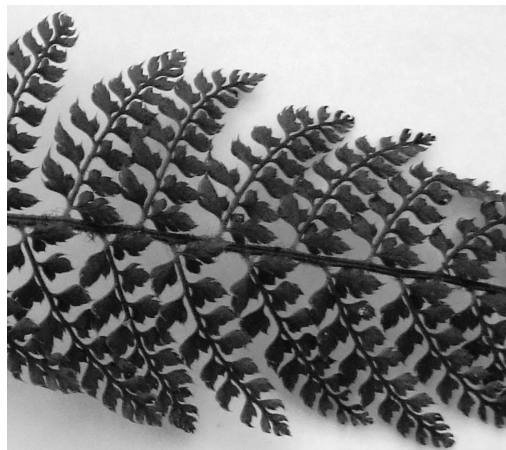


Fig. 1 A fern leaf

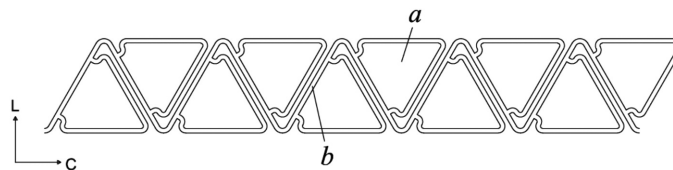
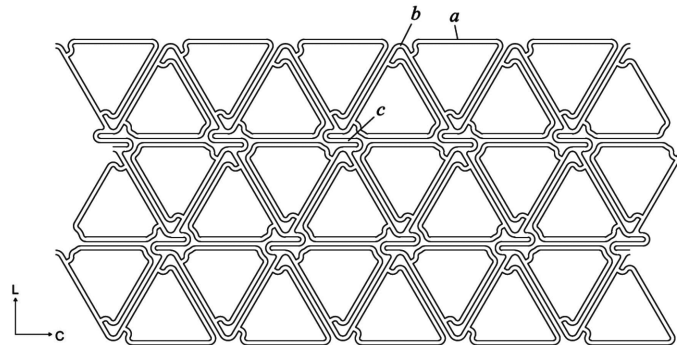


Fig. 2 The developed profile of a single ring of the leaf stent



Fig. 3 Folding procedure of a single ring

Fig. 4 An example of the leaf stent comprising three rings interconnected by *S*-shaped intermediate connection *c*

triangular in outer shape. The leaf components can either be solid leaves or modified to each comprise a frame defining a central aperture which is covered by other materials, e.g., a flexible membrane.

In principle, the leaf stent can comprise any number of chains of Fig. 2 in the longitudinal direction  $L$  and any number of leaf components  $a$  in the circumferential direction  $C$  in each chain. Fig. 4 shows an example of the stent comprising three chains each supporting ten leaf components  $a$ . Adjacent chains are interconnected to each other via *S*-shaped intermediate connection  $c$  each extending between the joint portions of the corresponding linkage components. In this example, there are five intermediate connections  $c$  between adjacent chains so that a closed-cell design is obtained. However, the number of intermediate connections  $c$  can be changed so that various mechanical properties of the stent can be achieved. The closed-cell design provides a minimum gap between adjacent chains when the stent is curved, whereas using fewer number of intermediate connections  $c$ , i.e., the open-cell designs, can produce better longitudinal flexibility. Fig. 5 shows a second example of the leaf stent which comprises three chains interconnected by the intermediate connections  $d$ . Instead of connecting the joint portions of the linkage components, the intermediate connections  $d$  connect the corresponding leaf components in this example. When folded, the intermediate connections  $d$  change in orientation, as shown in Fig. 6. As a result, the distance between two chains in the longitudinal direction  $L$  does not experience much change in the folded and expanded states, keeping the overall change in the length of the stent before and after folding small. Arguably, the intermediate connection design of the second example has two advantages. First, the nominal length of each intermediate connection  $d$  is maximized so that the stent has a good longitudinal flexibility; second, the stent can have a uniform deformed shape under bending because the adjacent chains are fully connected by the intermediate connections  $d$ , which is similar to a closed-cell design.

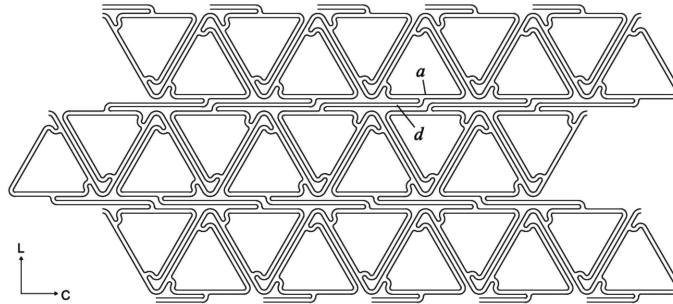


Fig. 5 An example of the leaf stent comprising three rings interconnected by intermediate connection  $d$

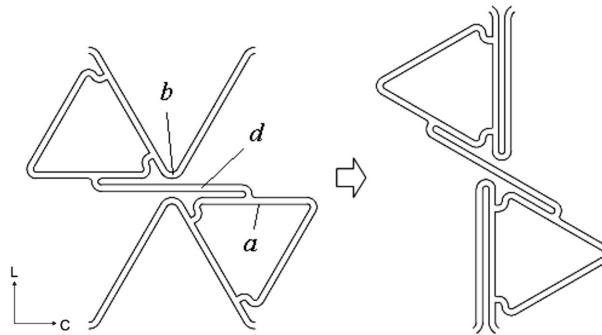


Fig. 6 Folding of the intermediate connections  $d$  in Fig. 5

### 3. Materials and methods in FEA

The finite element method was used to investigate the strain, radial force, longitudinal flexibility and stent-artery interaction of the leaf stent. The preferred material for the leaf stent is the superelastic nitinol. In the numerical models, it was assumed that the stent material was homogeneous and isotropic. Table 1 lists the material properties of nitinol used in the simulations which were obtained from Rebelo *et al.*'s paper (Rebelo *et al.* 2004). The finite element analysis was performed using ABAQUS/Standard version 6.7 (SIMULIA Inc., USA) due to its built-in user material subroutine suitable for modelling nitinol and its good capability to cope with problems involving large nonlinear deformations.

Table 1 Material properties of nitinol used in the simulations

Property	Value	Definition
$E_A$	50000 MPa	Austenite elasticity
$E_M$	37000 MPa	Martensite elasticity
$\sigma_M^s$	400 MPa	Starting transformation stress of loading
$\sigma_M^f$	650 MPa	End transformation stress of loading
$\sigma_A^s$	350 MPa	Starting transformation stress of unloading
$\sigma_A^f$	80 MPa	End transformation stress of unloading
$\varepsilon_L$	0.055	Maximum residual strain

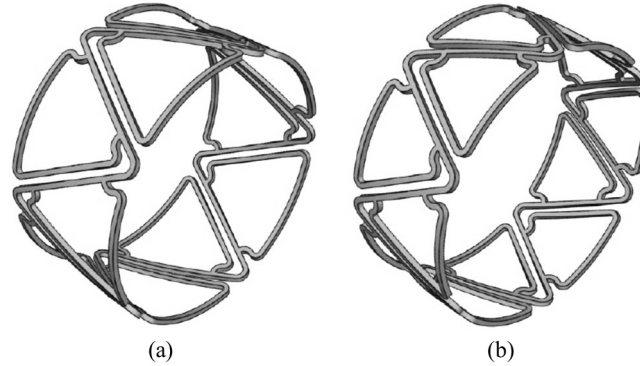


Fig. 7 (a) A single ring of the leaf stent supporting ten leaf components and (b) A single ring of the leaf stent supporting twelve leaf components

Table 2 Geometric parameters of eight models of the leaf stent

First group				
Model	A <sub>5</sub>	B <sub>5</sub>	C <sub>5</sub>	D <sub>5</sub>
$t$ (mm)	0.075	0.05	0.05	0.05
$w$ (mm)	0.075	0.075	0.075	0.05
$w_f$ (mm)	0.075	0.075	0.05	0.05
Second group				
Model	A <sub>6</sub>	B <sub>6</sub>	C <sub>6</sub>	D <sub>6</sub>
$t$ (mm)	0.075	0.05	0.05	0.05
$w$ (mm)	0.075	0.075	0.075	0.05
$w_f$ (mm)	0.075	0.075	0.05	0.05

### 3.1 Strain analysis

Eight structural models, divided into two groups, were considered for the strain analysis of the leaf stent. Models A<sub>5</sub>, B<sub>5</sub>, C<sub>5</sub> and D<sub>5</sub> are single rings of the stent each supporting ten leaf components, as shown in Fig. 7(a), whereas each of models A<sub>6</sub>, B<sub>6</sub>, C<sub>6</sub> and D<sub>6</sub> supports twelve leaf components, as shown in Fig. 7(b). The geometric parameters of the models are listed in Table 2, where variables  $t$ ,  $w$  and  $w_f$  are defined in Fig. 8. All the models have an initial radius of 2 mm, a typical value for the radius of a brain stent in the expanded state. During simulation, each model was crimped to a minimum radius of 0.5 mm, corresponding to the fully packaged state, and the maximum strain in the folded state was obtained. Each stent model was meshed with 8-node linear brick elements defined with reduced integration and hourglass control. The numbers of nodes and elements used to mesh each model are listed in Table 3.

To simulate the crimping procedure, a cylinder that was aligned with the axis of the model was used to apply an external pressure which compressed the model in the radial direction. The ABAQUS user subroutine RSURFU was used to prescribe such an analytical cylinder with a single parameter describing the radius. Contact between the model and the cylinder was modelled using an exponential pressure-overclosure constraint, in which the contact pressure increases exponentially as the clearance decreases. This defined a softened contact relationship that prevented excessive mesh

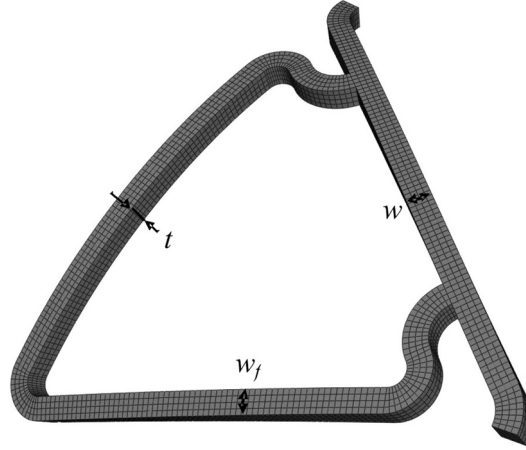

 Fig. 8 Definitions of  $t$ ,  $w$  and  $w_f$ 

Table 3 Geometric parameters of eight models of the leaf stent

Model	A <sub>5</sub>	B <sub>5</sub>	C <sub>5</sub>	D <sub>5</sub>
Nodes	94001	94001	80651	81201
Elements	60320	60320	49800	50120
Model	A <sub>6</sub>	B <sub>6</sub>	C <sub>6</sub>	D <sub>6</sub>
Nodes	93001	93001	82741	80281
Elements	59712	59712	51072	49584

distortion, which, otherwise, could have been generated by a hard contact. As the cylinder radius was decreased, it displaced the model radially, applying a compressive load without imposing additional constraints. The model was free to slide and lift off the inner surface of the cylinder, thereby accurately representing folding of the structure. Rigid body motion was eliminated by fixing the nodes at the extreme longitudinal positions at one end of the model in both longitudinal and circumferential directions.

### 3.2 Radial force

The radial force of the leaf stent was investigated by first crimping the stent from the expanded state to the fully folded state using the same approach described above and then deploying the stent inside another cylinder with a fixed radius smaller than the initial radius of the stent. The cylinder in which the stent was deployed was meshed with SMF3D4R i.e., a 4-node quadrilateral surface element. All nodes on the meshed cylinder were constrained in both longitudinal and circumferential directions and prescribed to have the same radial displacement as a reference point located on the cylinder by using the multipoint constraint in ABAQUS. The radius of the cylinder was then fixed by fixing the reference point at a certain radial position. It was found that the scalar summation of the contact forces  $\Sigma F_c$  between the stent and the inner side of the meshed cylinder was equal to the radial reaction force  $F_{ref}$  applied to the reference point. On the other hand,  $\Sigma F_c$  was equal to the hoop force of the stent  $f_\theta$  multiplied by  $2\pi$ . Consequently, the relationship between the radius and the hoop force of the stent could be obtained by deploying the stent inside a series of such cylinders

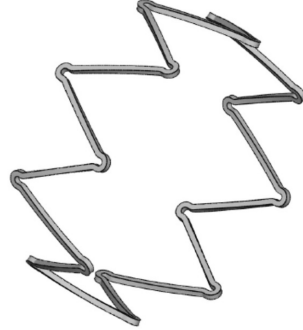


Fig. 9 A single ring of the Neuroform stent

with radii ranging from 0.5 to 2 mm and measuring the radial reaction forces  $F_{\text{ref}}$  at the reference points. The same eight models listed in Table 2 were considered. In addition, the radial forces of the eight models were compared to that of a single ring of the Neuroform stent (Boston Scientific, USA), as shown in Fig. 9. The strut width  $w$  and thickness  $t$  of the Neuroform stent were made the same as those of models  $A_5$  and  $A_6$  for comparison. A single ring of the Neuroform stent has eight crowns whereas models  $A_5$  and  $A_6$  have only five and six crowns, respectively.

### 3.3 Longitudinal flexibility

The longitudinal flexibility was compared among five stent designs, as shown in Fig. 10, where stent I comprises six rings of model  $A_5$  interconnected by *S*-shaped intermediate connections with a

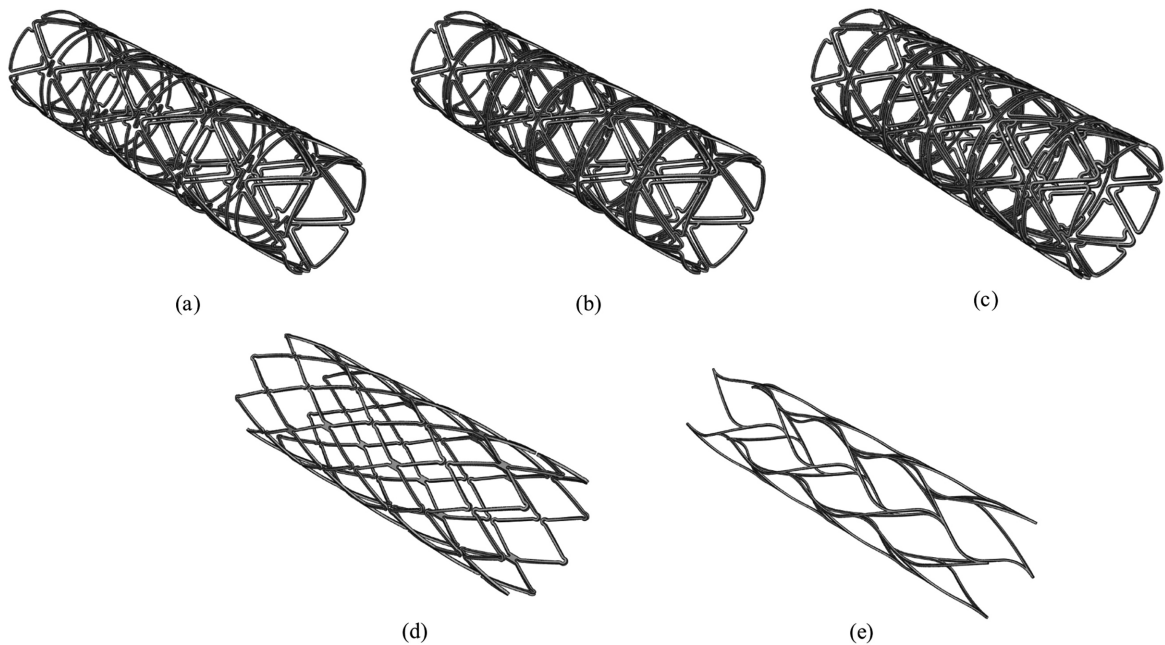


Fig. 10 Five stent models considered for longitudinal flexibility. (a)-(c) Stents I, II and III, (d) The Neuroform stent and (e) The Enterprise stent

closed-cell design, stent II comprises six rings of model A<sub>5</sub> connected by intermediate connections of Fig. 5, stent III consists of six rings of model A<sub>6</sub> connected by intermediate connections of Fig. 5, and the rest are respectively replications of the Neuroform stent and the Enterprise stent (Cordis, USA). Similarly, the strut width  $w$  and thickness  $t$  of Stent IV and V were taken to be the same as those of models A<sub>5</sub> and A<sub>6</sub> for comparison. The widths of the intermediate connections of Stents I to III are all 0.05 mm.

To simulate the bending of the stent, the nodes at the extreme longitudinal positions at each end of the stent were attached to a rigid plane whose reference point was located on the central axis of the stent and had a single translational degree of freedom along the axis. A bending load was applied to the stent by gradually rotating the reference points of the rigid plates in opposite directions until the curvature of the stent reaches  $0.1 \text{ mm}^{-1}$ . Results are expressed in terms of bending moment against curvature.

### 3.4 Stent-artery interaction

Finally, to investigate the interactions between the leaf stents and the arteries, the eight models listed in Table 2 were deployed inside an idealized straight artery model, whose length, internal diameter and wall thickness equal 6, 3.2 and 0.5 mm, respectively. A linear elastic material property was modelled for the artery with the Young's modulus of 1.365 MPa and the Poisson's ratio of 0.27 (Rebelo *et al.* 2009). The artery was meshed with 8-node continuum shell elements SC8R. Crimping and deployment of each model were controlled by a user-defined analytical surface as described previously. A softened contact with an exponential pressure-overclosure relationship was defined between the stent models and the internal surface of the artery. No contact was defined between the analytical surface and the artery so that the analytical surface penetrated the artery as it expanded radially. The stresses in the artery wall were measured.

## 4. Results and discussion

### 4.1 Strain analysis

It is important to ensure that during folding, the maximum strain in the stent does not exceed 8%, the maximum recoverable strain of nitinol, so that the stent can completely recover its original shape upon expansion. Table 4 shows the maximum equivalent uniaxial strains  $\epsilon_{\max}$  of the eight models in the fully folded state. Note that all the strains are smaller than 8%, meaning that the models do not experience plastic deformation during folding. Models with 10 leaf components have less strain than that of the corresponding models with 12 leaf components. Therefore, designs with fewer leaves should be adopted if the strain level of the stent needs to be reduced. Furthermore, the

Table 4 Maximum equivalent uniaxial strains of the eight models in the folded state

Model	A <sub>5</sub>	B <sub>5</sub>	C <sub>5</sub>	D <sub>5</sub>
$\epsilon_{\max}$	7.43%	7.24%	6.59%	5.13%
Model	A <sub>6</sub>	B <sub>6</sub>	C <sub>6</sub>	D <sub>6</sub>
$\epsilon_{\max}$	7.46%	7.56%	7.41%	6.04%

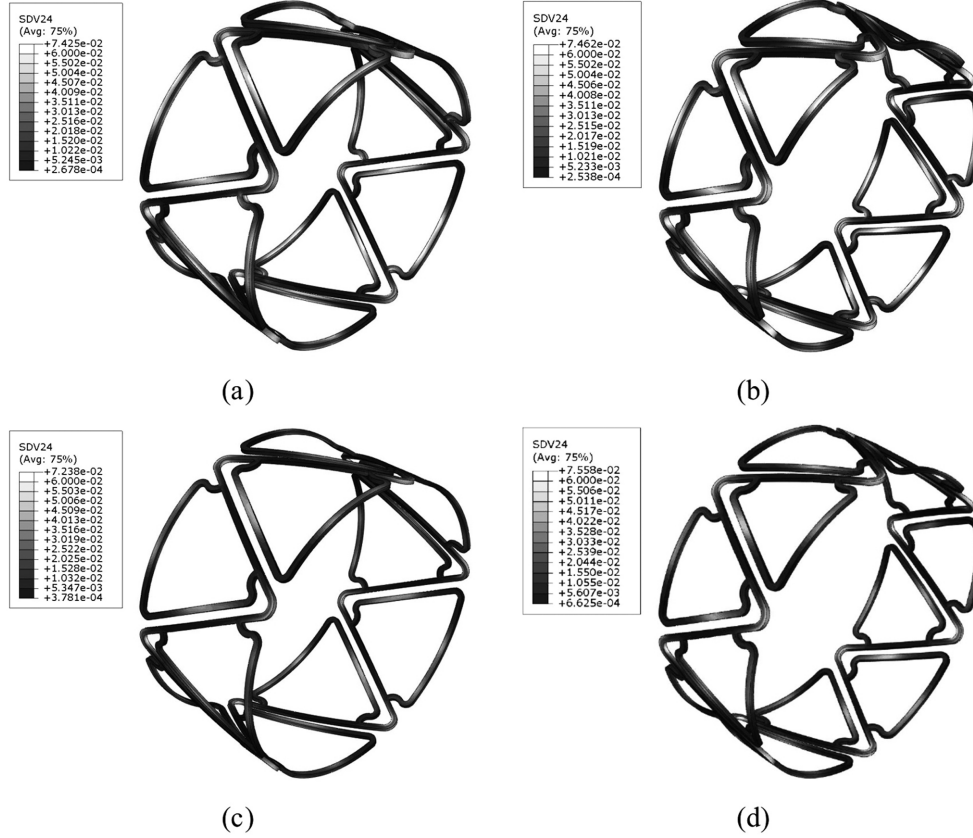


Fig. 11 Strain contour maps of the folded states of models (a)  $A_5$ , (b)  $A_6$ , (c)  $B_5$  and (d)  $B_6$ . Plotted on the expanded shapes for clarity

results show that reducing width  $w$  and/or  $w_f$  of the strut reduces the maximum strain whereas reducing wall thickness  $t$  does not necessarily reduce the maximum strain as the maximum strain of model  $B_6$  is even greater than that of model  $A_6$ . Nevertheless, reducing the wall thickness  $t$  is helpful in terms of reducing the strain level in the frame of the leaf components, as illustrated in Fig. 11, in which the strain contour of the folded state of each model is plotted on the undeformed shape for clarity. High strain regions with a strain level greater than 6% are plotted with red colour. Note that models  $A_5$  and  $A_6$  have substantial high strain regions in the frames according to Figs. 11(a) and (b). However, when wall thickness  $t$  of the models is reduced to 0.05 mm, no high strain region is found in the frames in both models as shown in Figs. 11(c) and (d).

#### 4.2 Radial force

Fig. 12 plots the hoop forces per unit length against the radius of the models. According to Fig. 12, the radial force of the overlap stent can be divided into two stages. At the first stage when the radius of the stent is smaller than 1mm, the hoop force decreases sharply from a relatively high value in the folded state. A close examination reveals that at this stage the frames of each model are curved to accommodate the small radius and thus the radial force is highly affected by the

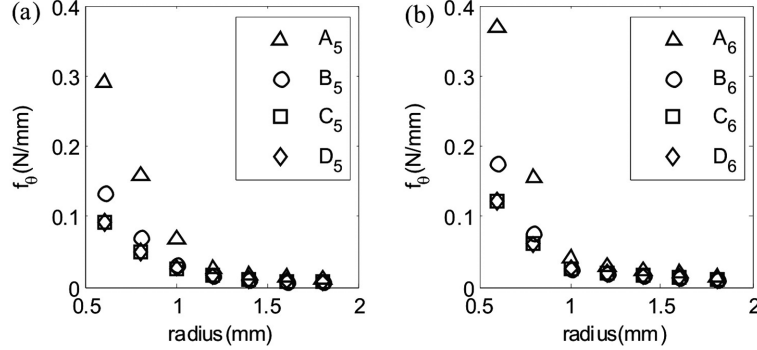

 Fig. 12 Hoop forces per unit length against radius, (a) models A<sub>5</sub>, B<sub>5</sub>, C<sub>5</sub> and D<sub>5</sub> and (b) models A<sub>6</sub>, B<sub>6</sub>, C<sub>6</sub> and D<sub>6</sub>

Table 5 Hoop forces of the eight models when the radius equals 1.6 mm

Model	A <sub>5</sub>	B <sub>5</sub>	C <sub>5</sub>	D <sub>5</sub>
$f_{\theta} _{R=1.6\text{mm}}$ (N)	0.165	0.103	0.102	0.043
$S_c \times w$ (mm <sup>3</sup> )	4.2E-4	2.8E-4	2.8E-4	1.2E-4
Model	A <sub>6</sub>	B <sub>6</sub>	C <sub>6</sub>	D <sub>6</sub>
$f_{\theta} _{R=1.6\text{mm}}$ (N)	0.192	0.125	0.124	0.050
$S_c \times w$ (mm <sup>3</sup> )	4.2E-4	2.8E-4	2.8E-4	1.2E-4

deformation of the frames. As a result, models C<sub>5</sub> and D<sub>5</sub> have roughly the same radial force in this stage and so do models C<sub>6</sub> and D<sub>6</sub> because the frames of these models have the same width  $w_f$  and thickness  $t$ . At the second stage when the radius is greater than 1mm, the hoop force is much lower in comparison with that at the first stage and the change of the hoop force as a function of the radius is much smoother as well. This is because as the radius of the stent increases, the frames recover to their original shape and the strains in the frames are mostly released. Because the frames are allowed to slide freely in the circumferential direction, they do not contribute to the radial force. Therefore, the radial forces of the overlap stents at the second stage are mainly determined by the strut geometries of the linkage components. Table 5 lists the hoop forces of the eight models when the radius is 1.6 mm. Note that the hoop force is roughly proportional to  $S_c \times w$ , where  $S_c = w \times t$ , is the cross-sectional area of the strut. Models B<sub>5</sub> and C<sub>5</sub> have the same hoop force and so do models B<sub>6</sub> and C<sub>6</sub> because these models have the same  $S_c \times w$ . If considering the linkage components alone, the models are respectively equivalent to typical 5-crown and 6-crown zig-zag rings. Further numerical simulations on the zigzag rings which are not described here for brevity showed that a six-crown zigzag ring has the higher radial stiffness than a 5-crown counterpart and more generally a zigzag ring with more crowns has higher radial stiffness. The same pattern can be observed in Table 5, which further proves that the radial force of the leaf stent at the second stage is determined by the linkage components.

Fig. 13 compares the radial forces of models A<sub>5</sub> and A<sub>6</sub> with that of a single ring of the Neuroform stent (Boston Scientific, MA, USA) which has been successfully used for the intracranial aneurysm and thus can serve as a benchmark. Note that the hoop forces of models A<sub>5</sub> and A<sub>6</sub> are much higher than that of the Neuroform stent at small radius due to the deformation of the leaves. This effect quickly dissipates, though. The hoop forces soon enter a plateau region. In this region, they are

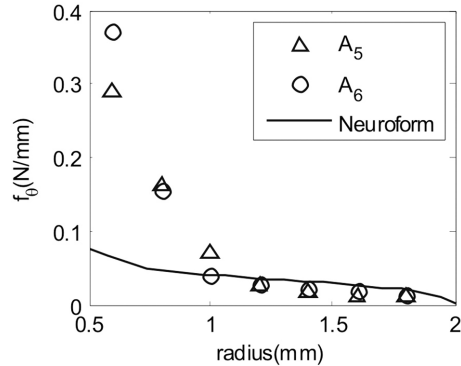


Fig. 13 Hoop forces per unit lengths of models  $A_5$  and  $A_6$  and the Neuroform stent

slightly smaller than that of the Neuroform stent because the Neuroform stent has a higher number of crowns, as discussed previously, but the difference among them remains small. Unlike the coronary stent for which a high radial strength is desired to keep the blocked artery open, the stent used for the direct treatment of intracranial aneurysms only needs a moderate radial stiffness that is enough to prevent migration of the stent within the artery. A too high radial force, on the other hand, may cause potential damage to the artery. Therefore, a radial force which is comparable to that of the Neuroform stent as observed in the plateau region of the present examples of the leaf stent justifies the applicability of the stents in the brain. Meanwhile, the results also suggest that deployment of the leaf stent in or early contact of the stent with small arteries (i.e., for the present examples, an artery smaller than 1 mm in radius) should be avoided.

#### 4.3 Longitudinal flexibility

The bending moment versus curvature curves of the five model stents are plotted in Fig. 14,

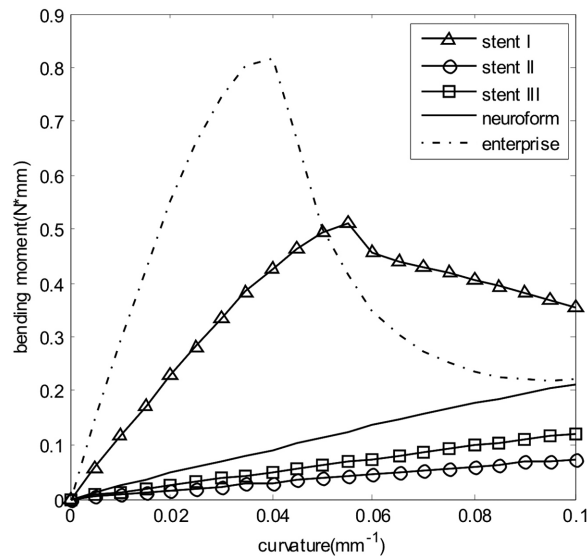


Fig. 14 Bending moment versus curvature curves of five models in Fig. 10

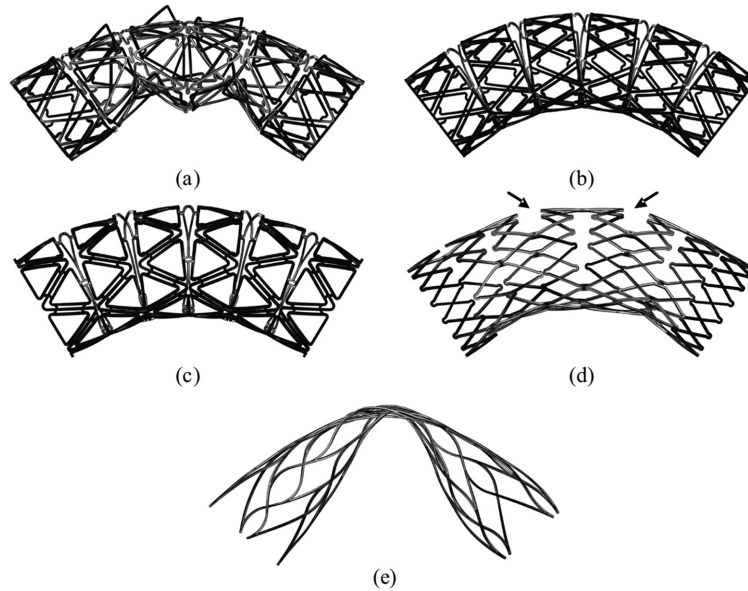


Fig. 15 Deformed shapes of the five models under the maximum bending moment, (a)-(c) Stents I, II and III, (d) The Neuroform stent and (e) The Enterprise stent

where the triangle, circle, square, solid and dash-dotted lines correspond to the leaf stents I, II and III, as well as the Neuroform stent and the Enterprise stent, respectively. Note that the leaf stents with the intermediate connections shown in Fig. 5, i.e., stents II and III, have the better longitudinal flexibility than the Neuroform stent which again serves as a benchmark. Although the leaf stent with the *S*-shaped intermediate connections, i.e., stent I, is stiffer than the Neuroform stent, it still has a good flexibility in comparison with the Enterprise stent, another commercially available stent used for stent assisted coiling. Note that sudden changes occur at certain points in the bending moment and curvature curves of both stent I and the Enterprise stent. Beyond those points the bending moments decrease as the curvature increases. This is due to the buckling of the stents which causes the stent to lose the circular profile. The Enterprise stent buckles earlier than stent I. No buckling was observed in the other three stents throughout the curvature variation range under consideration. Furthermore, it was found that stent II is more flexible than stent III, meaning that the leaf stent with fewer leaf components circumferentially has a better longitudinal flexibility.

Fig. 15 shows the deformed shapes of the five stents under the maximum bending moment. It is obvious that both stent I and the Enterprise stent buckled, as discussed above. The Neuroform stent produces an uneven deformed shape with large gaps appearing between adjacent rings (see the arrows) due to its open-cell design. The deformed shapes of stent II and III are quite uniform, thus providing a good and even coverage along the stent.

#### 4.4 Stent-artery interaction

Fig. 16 shows the Von Mises stress contour maps and the maximum Von Mises stresses exerted on the artery within which the stents are deployed. The first eight sub figures correspond to the results generated by the eight models listed in Table 2, whereas Fig. 16(i) is the artery holding a single ring of the Neuroform stent. Note that all the eight models of the leaf stent produce smaller

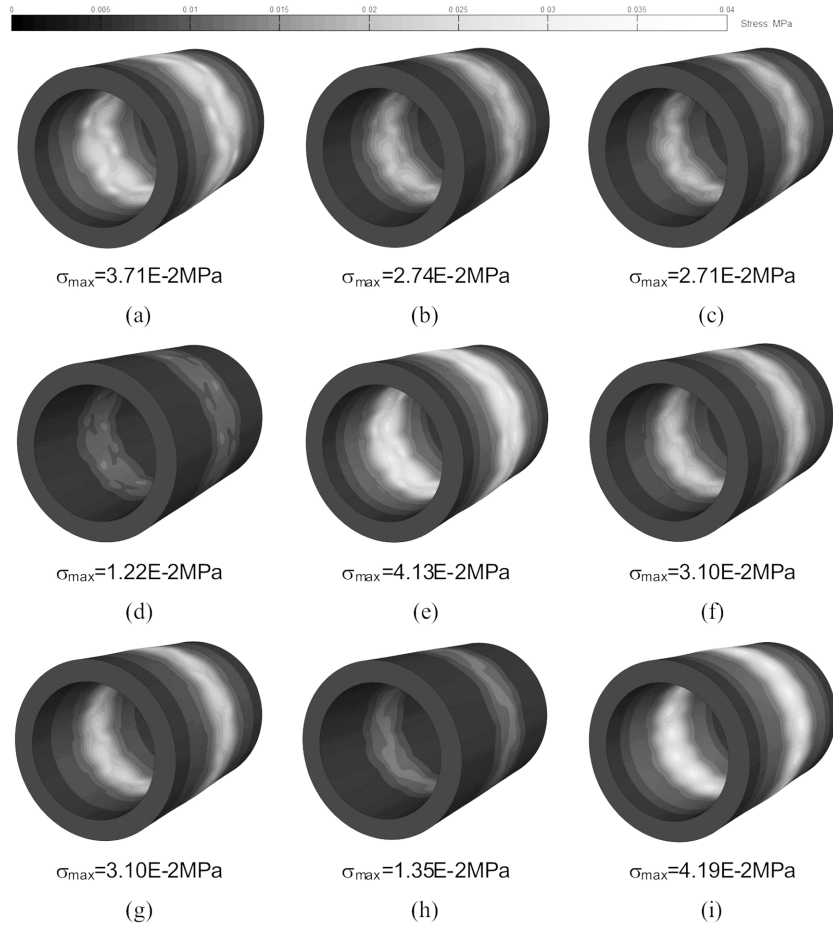


Fig. 16 Von Mises stress contour maps on the artery within which the stents are deployed. (a)-(d) Models A<sub>5</sub>, B<sub>5</sub>, C<sub>5</sub> and D<sub>5</sub>, (e)-(h) models A<sub>6</sub>, B<sub>6</sub>, C<sub>6</sub> and D<sub>6</sub>, and (i) the Neuroform stent

stresses on the artery than that produced by the Neuroform stent, indicating that the leaf stent will not cause harm to the artery as long as the Neuroform stent does not. By comparing the results among the eight models, it was found that models with five leaf components produce smaller stress on the artery than what the six-leaf counterparts do. Furthermore, the stress on the artery gets smaller as the  $S_c \times w$  reduces. All these findings are comparable to the patterns found in the radial force.

## 5. Conclusions

An innovative stent design for the direct treatment of the intracranial aneurysm are presented in this paper. The stent is composed of a plurality of triangular leaf components attached to a zig-zag ring. The crimping of the stent is carried out by the deformation of the ring while the leaf components are wrapped around the ring and each other. The stent provides a high surface coverage with an average coverage rate of around 89% providing a 0.1 mm slot width between struts.

The mechanical properties of the leaf stent were studied using finite element method. It was shown that the strain level in the leaf stent is smaller than the maximum recoverable strain of nitinol. The radial force of the leaf stent is divided into two stages. In the first stage, the stent has a relatively high radial force compared to that of the Neuroform stent. In the second stage, the radial force of the leaf stent is in the same magnitude as that of the Neuroform stent. According to the findings, we define the second stage as the feasible design region of the leaf stent to prevent excessive pressure to the artery. The longitudinal flexibility of the leaf stent with the S-shaped intermediate connections is better than the Enterprise stent but poorer than the Neuroform stent, whereas the leaf stent with the other intermediate connections is more flexible than the Neuroform stent. In addition, the leaf stent can produce a uniform deformed shape while subjected to bending. This feature is not currently possessed by the Neuroform stent due to its open-cell design. A uniform deformed shape is beneficial to provide a better coverage. Finally, the stress in the artery wall as the result of placement of the leaf stent within the artery is compared to that of the Neuroform stent. It was found that the leaf stent produces smaller stress in the artery than the Neuroform stent does.

The leaf stent is designed for direct treatment of intracranial aneurysms without coils. The numerical simulation has shown that the current design is viable and has performance features superior to the open-cell cerebral stents while at the same time provide sufficient coverage to shut the aneurysm.

A number of leaf stents have been produced from nitinol tubes and experimental work, including crimping and mechanical tests, is underway and will be reported in due course.

## Acknowledgements

The authors also wish to thank the Oxford University Supercomputing Centre for providing access to their supercomputer for performing the finite element analysis presented in this paper.

## References

- Fiorella, D., Albuquerque, F.C., Deshmukh, V.R., Woo, H.H., Rasmussen, P.A., Masaryk, T.J. and McDougall, C.G. (2006), "Endovascular Reconstruction with the Neuroform Stent as Monotherapy for the Treatment of Uncoilable Intracranial Pseudoaneurysms", *Neurosurgery*, **59**(2), 291-300.
- Brisman, J.L., Song, J.K. and Newell, D.W. (2006), "Cerebral Aneurysms", *N. Engl. J. Med.*, **355**(9), 928-939.
- Kim, M., Taulbee, D.B., Tremmel, M. and Meng, H. (2008), "Comparison of two stents in modifying cerebral aneurysm hemodynamics", *Ann. Biomed. Eng.*, **36**(5), 726-741.
- Mitha, A.P. and Ogilvy, C.S. (2005), "ISAT: coiling or clipping for ruptured intracranial aneurysms?", *Lancet Neurol.*, **4**(12), 791-792.
- Rebelo, N., Fu, R. and Lawrenchuk, M. (2009), "Study of a nitinol stent deployed into anatomically accurate artery geometry and subjected to realistic service loading", *J. Mater. Eng. Perform.*, **18**(5-6), 655-663.
- Rebelo, N., Gong, X., Hall, A., Pelton, A.R. and Duerig, T.W. (2004), "Finite element analysis on the cyclic properties of superelastic nitinol", ABAQUS Users' Conference, 601-613.
- Wijdicks, E.F.M., Kallmes, D.F., Manno, E.M., Fulgham, J.R. and Piepgras, D.G. (2005), "Subarachnoid hemorrhage: neurointensive care and aneurysm repair", *Mayo. Clin. Proc.*, **80**(4), 550-559.
- Zhou, X., You, Z. and Byrne, J. (2009), Stent, British Patent Application 0900565.3.